molecular pharmaceutics

pubs.acs.org/molecularpharmaceutics Article

In Situ Monitoring of Protein Unfolding/Structural States under Cold High-Pressure Stress

Diana C. Gomes, Susana C. M. Teixeira, Juscelino B. Leão, Vladimir I. Razinkov, Wei Qi, Miguel A. Rodrigues, and Christopher J. Roberts*

Cite This: *Mol. Pharmaceutics* 2021, 18, 4415−4427 Read Online

ACCESS | Metrics & More | Article Recommendations | Supporting Information

ABSTRACT: Biopharmaceutical formulations may be compromised by freezing, which has been attributed to protein conformational changes at a low temperature, and adsorption to ice−liquid interfaces. However, direct measurements of unfolding/conformational changes in sub-0 °C environments are limited because at ambient pressure, freezing of water can occur, which limits the applicability of otherwise commonly used analytical techniques without specifically tailored instrumentation. In this report, small-angle neutron scattering (SANS) and intrinsic fluorescence (FL) were used to provide *in situ* analysis of protein tertiary structure/folding at temperatures as low as −15 °C utilizing a high-pressure (HP) environment (up to 3 kbar) that prevents water from freezing. The results show that the α-chymotrypsinogen A (aCgn) structure is reasonably maintained under acidic pH (and corresponding pD) for all conditions of pressure and temperature tested. On the other hand, reversible structural changes and formation of oligomeric species were detected near −10 °C via HP-SANS for ovalbumin under neutral pD conditions. This was found to be related to the proximity of the temperature of cold denaturation of ovalbumin (T_{CD} ∼ −17 °C; calculated via isothermal chemical denaturation and Gibbs−Helmholtz extrapolation) rather than a pressure effect. Significant structural changes were also observed for a monoclonal antibody, anti-streptavidin IgG1 (AS-IgG1), under acidic conditions near −5 °C and a pressure of ∼2 kbar. The conformational perturbation detected for AS-IgG1 is proposed to be consistent with the formation of unfolding intermediates such as molten globule states. Overall, the *in situ* approaches described here offer a means to characterize the conformational stability of biopharmaceuticals and proteins more generally under cold-temperature stress by the assessment of structural alteration, self-association, and reversibility of each process. This offers an alternative to current *ex situ* methods that are based on higher temperatures and subsequent extrapolation of the data and interpretations to the cold-temperature regime.

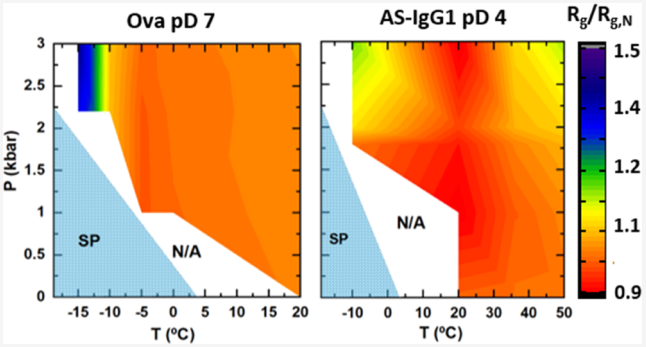

KEYWORDS: *protein denaturation, folding, conformational stability, subzero temperature, pressure, in situ approaches, small-angle neutron scattering, fluorescence spectroscopy*

1. INTRODUCTION

Cold temperature chains (refrigerated and subzero regimes) are currently the preferred best option to prolong the shelf-life of therapeutic protein solutions, as well as to assure protein stability during the transfer of bulk drug substance to drug product facilities.[1,2] That notwithstanding, cold-induced denaturation is expected to occur at a sufficiently low temperature (T) and thereby accelerate unwanted protein−protein association events over a long-term storage period.[3,4] To this end, understanding protein structural changes under different stresses can be used as an indicator of protein conformational stability and aggregation propensity during formulation development stages.[5−9]

From a practical standpoint, protein conformational stability under cold-temperature conditions can be marginal, as the free energy change for for the equilibrium folding−unfolding transition of a given protein or protein domain (ΔG_{un}, $G_{unfolded} - G_{folded}$) may be only tens of kJ/mol (a few kcal/mol) and the midpoint temperature of cold denaturation (T_{CD}) may not be far below 0 °C. Measurements of unfolding and structural changes under cold-temperature conditions are important to help define a given protein stability curve under selected storage conditions. This can be difficult to implement at temperatures where cold unfolding events typically occur (e.g., below the atmospheric freezing point for water).[4,10−12]

Received: July 29, 2021
Revised: October 12, 2021
Accepted: October 13, 2021
Published: October 26, 2021

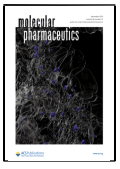

Standard experimental approaches for accelerating aggregation and assessing conformational stability are often questioned as they are performed under high-temperature conditions—e.g., via isothermal chemical denaturation (ICD) and thermal scanning experiments—and then need to be extrapolated over large temperature ranges and/or large denaturant concentration ranges to assess conformational stability under cold-temperature conditions.[13,14] This can lead to ambiguous correlations between protein unfolding and non-native aggregation under desired storage conditions.[15,16] This is also the case if ICD methods neglect potential aggregation triggered by partial/full denaturation events (e.g., inaccurate assumption of a reversible two-state unfolding).[17]

Protein domains that are prone to unfold or partially unfold may differ when compared between high- and low-temperature regimes, as the balance between stabilizing and destabilizing factors can be different.[18,19] Some unfolding states may retain a higher degree of secondary structure (often called molten globule states), and this has been associated with the cold-temperature regime.[20,21] This is not always the case as others have demonstrated that high-temperature stress can also induce intermediary states with different secondary structural features.[22−24] Furthermore, for multidomain proteins such as monoclonal antibodies (MAbs), the unfolding process usually follows multiple cooperative transitions[13] (includes intermediary unfolded species), which involves independent or coordinated unfolding of domains.

An *in situ* approach would enable one to circumvent extrapolation of analysis of protein unfolding/conformational states and help to capture intermediary states that may differ over a broad temperature range. However, being able to directly track folding equilibria and structural changes under sub-0 °C conditions requires using an approach that prevents freezing of the solvent. Particularly, freezing brings many other complex aspects that may impact protein structure (e.g., ice−liquid interfacial stress, cryo-concentration, shifts of pH if buffer species crystallize, etc.).[25−29] There are multiple options to decrease the freezing point of a given protein solution. One is to increase the concentration of co-solutes (i.e., colligative effects), while another is to increase the hydrostatic pressure (P). The latter offers an important advantage as pressure is usually considered a moderate denaturant. In most cases, for reasonably stable monomeric proteins, no major changes in the folding equilibrium are expected at intermediate-pressure conditions (below ca. 2−3 kbar).[30] Nevertheless, both pressure and cold temperature can induce important subtle protein structural changes,[24,31−33] and deconvolution of each individual effect may be challenging.

Pressure-mediated unfolding and aggregation have been a focus of recent and earlier studies, as elevated pressure effects can shed light into protein structure-related processes such as (re)folding, ligand binding, misfolding, and dissociation events.[34−36] Pressure-induced unfolding is driven, in part, by the packing of the protein structure as the solvent-excluded cavities become solvated.[30,37,38] The outcome is disruption of protein tertiary/quaternary structure at lower pressures, while secondary structural features are affected at sufficiently higher pressures.[30] The majority of pressure-induced unfolding studies have focused on globular proteins above 0 °C.[24,31,39,40] As noted above, MAbs are more complex than typical monomeric proteins and typically follow multistate denaturation processes. The effect of elevated pressure on MAbs has been explored in a few cases, but typically only near room-temperature conditions.[41]

For the present study, two globular proteins (α chymotrypsinogen A, aCgn, at pH 4.5, and ovalbumin, Ova, at pH 7 or the equivalent pD value) and a model MAb (anti-streptavidin IgG1, AS-IgG1, at pH 4, or the equivalent pD value) were tested systematically for structural changes as a function of pressure and (cold) temperature. These proteins are expected to offer different conformational behavior under high-pressure (HP) and temperature denaturing conditions as they span from globular to multidomain proteins.[42] The range of acidic to neutral pH to be tested has also shown to significantly impact protein denaturation states.[43−45] Small-angle neutron scattering (SANS) and intrinsic fluorescence (FL) techniques were used *in situ* under pressure conditions up to 3 kbar and temperatures down to −15 °C. This approach is shown to be attractive as a means to provide information under cold-temperature conditions regarding protein conformational changes. Particularly, *in situ* experimental methods can probe partially unfolded states and have the potential to improve current assessments/predictions of protein stability under cold storage without the need for extrapolation from higher-temperature conditions.

2. MATERIALS AND METHODS

2.1. Materials and Solution Preparation. The following buffers were prepared in distilled, deionized water (Milli-Q, resistivity 18.2 MΩ·cm, Millipore, Billerica, MA): 10 mM acetate at pH 4.5, 5 mM citrate at pH 4, 5 mM sodium phosphate at pH 7 (Fisher Scientific, Fair Lawn, NJ), and 10 mM histidine-HCl at pH 7 (Sigma-Aldrich, St. Louis, MO). Each buffer solution was titrated to the desired pH (±0.1) with 5 M sodium hydroxide solution (Fisher Scientific) or 5 M hydrochloric acid (Molecular Biology Grade, Fisher Scientific). All buffer solutions were filtered prior to use with 0.45 μm filters (Millipore).

Solutions of aCgn (Worthington Biochemical, Lakewood, NJ) prepared in sodium phosphate buffer at pH 7 at ∼30 mg/mL were treated with phenylmethylsulfonyl fluoride (PMSF, Sigma-Aldrich, St. Louis, MO) to deactivate potential residual proteases that become active at pH 5−7 in the commercial aCgn material, as previously described.[46] The phosphate buffer was replaced by 10 mM acetate at pH 4.5 via a dialysis step carried out for ∼48 h using a 10 kDa molecular-weight cutoff (MWCO) dialysis membrane (Spectra/Por 7, Spectrum Laboratories, Rancho Dominguez, CA). The buffer solution was replaced every 12 h. Afterwards, aCgn solutions were centrifuged at 3200 RCF for 15 min and filtered with 0.22 μm filters (Millipore).

Ova solutions were prepared by dissolving the lyophilized protein powder (Sigma-Aldrich, St. Louis, MO) in 10 mM histidine buffer at pH 7 at ∼20 mg/mL. A dialysis step was performed in 10 mM histidine buffer at pH 7. Stock AS-IgG1 solutions were supplied by Amgen (Thousand Oaks, CA) at a concentration of 30 mg/mL. Stock solution was dialyzed in 10 mM sodium citrate at pH 4. The dialysis procedure is the same as described above for aCgn solution. No further treatment steps were performed for both Ova and AS-IgG1 solutions.

Samples of each protein solution were prepared gravimetrically to the desired concentration using the respective buffer solution. Protein concentration was determined using a UV−vis spectrometer (Agilent 8453 UV−VIS, Agilent Technologies, Santa Clara, CA) at 280 nm with standard 10 mm

https://doi.org/10.1021/acs.molpharmaceut.1c00604
Mol. Pharmaceutics 2021, 18, 4415−4427

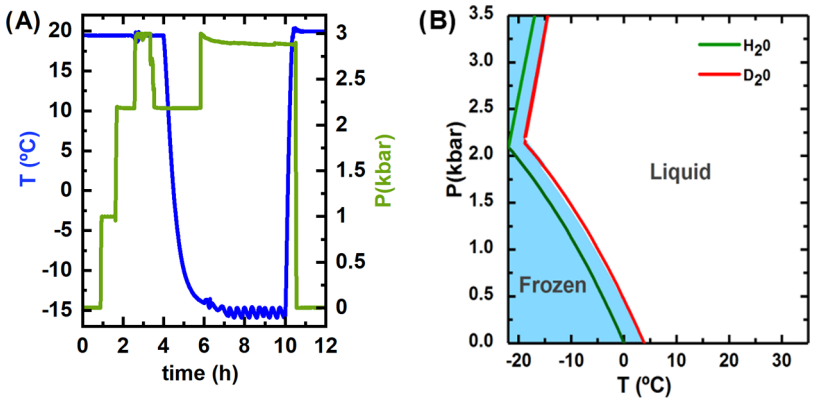

Figure 1. (A) Example of $P-T$ profiles recorded during an HP-SANS experiment. Temperature profiles are averaged from probes placed at the bottom and top of the HP cell, which is surrounded by a metal jacket. The Peltier system is placed at the base of the surrounding metal jacket. (B) Schematic representation of the P and T phase diagram of H_2O and D_2O as the solvent, assuming negligible freezing-point depression for the dilute dissolved solutes.

cuvettes. An average of three independent measurements were used to determine the final protein concentration. Extinction coefficients of 1.97,[47] 0.716,[48] and 1.586[49] mL/mg·cm were used to calculate the concentration of aCgn, Ova, and AS-IgG1, respectively.

Concentrated urea and guanidine hydrochloride stock solutions were prepared at 8 and 5 M, respectively, via dissolution of the denaturant (Fisher Scientific) in sodium acetate or histidine-HCl buffers. The final pH was adjusted with 5 M HCl. The refractive index and density of the urea stock solutions were taken into account to calculate the solution molarity.[50] Solutions of aCgn at 0.025 mg/mL were prepared with urea concentrations up to ∼7.5 M and incubated for a minimum of 3 h (time required to reasonably assure a folding−unfolding equilibrium) at a given temperature before starting the experiment. Reversibility of unfolding was evaluated for aCgn solutions at high concentrations of urea: buffer exchange steps were performed using 10 kDa MWCO Amicon-Ultra centrifugal tubes (Millipore) to remove the initial urea present in the solution and samples were retested.

Matching protein stock solutions were also prepared in deuterium oxide (D_2O—99.8% Cambridge isotope Lab, Inc., Tewksbury, MA) for use in SANS experiments. Buffer exchange steps were performed with the corresponding deuterated buffer that match the previously described H_2O-based buffers. The purification and dialysis steps were performed for aCgn solutions in the respective H_2O-based buffer before replacement by the deuterated buffer.

Buffer exchange steps were performed in Amicon-Ultra Centrifugal tubes (10 MWCO were used for aCgn and Ova solutions; 50 kDa MWCO were used for AS-IgG1) under refrigerated conditions (4 °C) to a final D_2O concentration of ∼99%. Final pD values were determined by measuring each solution pH value and using the following equation: pD = pH + 0.4.[51,52] Note that small deviations for the correction factor of 0.4 pH units have been reported and should be considered when comparing results in D_2O buffers.[53]

2.2. Controlled-Pressure Systems. Two different high-pressure (HP) cells were used for intrinsic fluorescence (FL) and small-angle neutron scattering (SANS) measurements. Structural and thermodynamic data were collected *in situ* for a given combination of temperature (down to −15 °C) and pressure (up to 3 kbar) to prevent water from freezing.

The HP-FL cell unit (ISS model HP-200)[54] was designed to be compatible with a variety of spectroscopic techniques. For the present work, the HP-FL cell unit was mounted on an adaptor customized by ISS to fit inside the sample compartment of an in-house Horiba Fluoromax 4 fluorometer (R928P photon counting PMT emission detector; scanning up to 80 nm/s; accuracy: 0.5 nm). A small-volume round quartz cuvette (volume requirement of ∼0.75 mL) was used as the sample container. A Teflon stopper was prepared to fit the cuvette bottleneck and positioned at 2/3 length from the top to allow enough travel distance when pressure is applied. The sample final volume takes into account the space in the stopper, which increases sample volume requirements to ∼1 mL. The pressurizing liquid used was ethanol (98% v/v). The temperature was controlled via an external bath circulator (PolyScience; model 40-A11B) that was directly attached to the HP-FL cell body unit; the cooling fluid used was a solution with a volume fraction of 50% water/ethylene glycol solution (freezing point is −36.5 °C) to access to the low-temperature range.

The HP-SANS cell unit used in this project was built at the National Institute of Standards and Technology (NIST) Center for Neutron Research (NCNR), in Gaithersburg, MD. This system is designed for studies of biological macromolecule solutions (BioSANS) over a broad temperature range, as described by Teixeira et al.[55] The sample volume requirement is ∼3 mL. Data were collected at a neutron wavelength of 6 Å and a wavelength spread of $\Delta\lambda/\lambda = 0.138$, covering a scattering vector amplitude range of $0.003 < q$ (Å^{-1}) < 0.25. Raw scattering data were corrected for transmission and scattering contributions from the solvent and the empty cell. The data were reduced to an absolute scale by normalizing the scattered intensity to the incident beam flux. The scattering profiles were scaled using the measured transmissions at each pressure, to account for changes in neutron pathlength (the HP-SANS cell design uses nonfixed windows) as well as the increased density of the solution under pressure.[56] Data reduction steps were performed using Igor Pro and the NCNR SANS reduction macros.[57] The cell temperature was controlled with a surrounding jacket thermalized with thermoelectric Peltier devices. Temperature profiles were recorded during the course of each run using four 100 Ω platinum resistance temperature sensors (Pt-100). Data collection was carried out in a vacuum-sealed chamber to

https://doi.org/10.1021/acs.molpharmaceut.1c00604
Mol. Pharmaceutics 2021, 18, 4415−4427

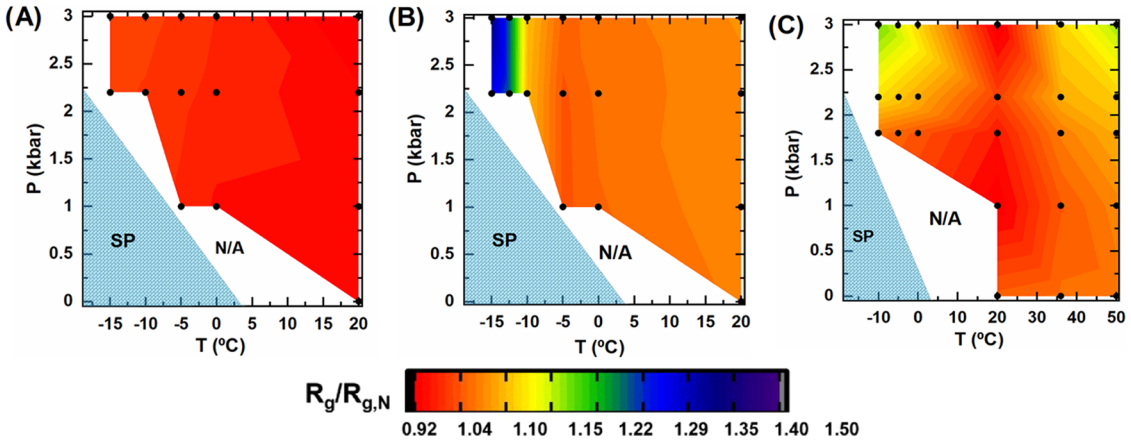

Figure 2. Surface plot representation of the ratio $R_g/R_{g,N}$ obtained from the Guinier approximation with SANS for each protein in an illustrative P/T phase diagram form: (A) aCgn, 10 mg/mL in 10 mM acetate buffer pD 4.5; (B) Ova 10 mg/mL in 10 mM histidine buffer pD 7; (C) AS-IgG1 5 mg/mL in 5 mM citrate buffer pD 4. $R_{g,N}$ values are set as the reference for each protein native state collected at 20 °C under atmospheric conditions: (A) 16.5 Å; (B) 23.1 Å; and (C) 45.8 Å. The scale is normalized to a 1.5-fold increase on $R_g/R_{g,N}$. Black circles represent the data points measured under a given temperature and pressure condition. The blue area represents the P/T conditions, where a pure D_2O solution is expected to be frozen (not drawn to scale). SP indicates solid phase. N/A indicates nonmeasured conditions.

prevent water condensation in the pressure cell during measurements at a low temperature.

An illustrative example of P/T profiles observed during the experiment is shown in Figure 1A: an equilibration time of ∼2.5 h was required to achieve the lowest temperature setpoint of −15 °C at 2.2 kbar. Figure 1B illustrates the P/T phase diagram for H_2O and D_2O as described elsewhere.[56] Combinations of pressure and cold temperature were chosen to prevent sample freezing. Note that the solid−liquid equilibrium line is expected to shift ∼3.8 °C for D_2O vs H_2O conditions.

For both HP-FL and HP-SANS, holding a given pressure of interest below −10 °C (P > 1.5 kbar to prevent sample freezing) is a known technical challenge. The relatively large volume of the pressure cells requires significant time to cool down and, as the cells adjusted to the heat removal, contraction of components occurs. The experiments were restarted if the system leaked. Detailed information on data analysis is provided in the Supporting Information.

3. RESULTS AND DISCUSSION

HP-FL and HP-SANS techniques were used to assess protein unfolding thermodynamics and structural changes as the temperature was reduced from room-/high-temperature conditions to sub-0 °C conditions. Three proteins, which differ in size, structure, and relative (high temperature) conformational stability, were chosen for comparison at neutral to acidic solution conditions: aCgn,[23,47,58−61] Ova,[62−66] and AS-IgG1.[49,67−69]

As a first step, changes in protein size were obtained via determination of the radius of gyration (R_g) from the HP-SANS scattering profiles for each protein. Figure 2 shows the average protein size as a function of pressure and temperature for all conditions tested, based on the Guinier approximation (see also the Supporting Information) for aCgn (Figure 2A), Ova (Figure 2B), and AS-IgG1 (Figure 2C). The contour plots provide a means to map the compactness of a given folding state for a broad range of pressure and temperature conditions; the particular combinations of pressure and temperature were selected so as to prevent sample freezing (the $P-T$ phase diagram is illustrated in Figure 1B). Complementary HP-SANS profiles and the corresponding R_g values were also collected for AS-IgG1 under high-temperature conditions (T up to 50 °C). The results show that the R_g values increase slightly for aCgn, and more significantly for Ova and AS-IgG1 compared with the corresponding native state values. The R_g values for the native or unstressed conditions ($R_{g,N}$) were obtained as a reference radius for the native solution structure at 20 °C under atmospheric conditions. The scale shown in Figure 2 is normalized to a maximum of 1.5-fold increase for $R_g/R_{g,N}$.

Overall, the aCgn monomer size remained relatively unchanged over the range of conditions tested (Figure 2A), while an increase in protein size is observed for Ova (Figure 2B) and AS-IgG1 (Figure 2C) for pressures higher than ∼2 kbar as temperature decreases to −15 and −10 °C, respectively. This suggests that conformational changes of Ova and AS-IgG1 result in a more expanded or unfolded structure. The same trend was observed for AS-IgG1 over the high temperature for pressures higher than 2 kbar.

Normalized Kratky plots (NKP)—normalized by the intensities at zero scattering angle, $I(0)$, and scaled by R_g—were used to compare the three different sized proteins in a common dimensionless scale (Figure 3). Overall, NKP profiles include information regarding size, shape, volume, and structure providing structural characterization for each protein under a given experimental condition.[70,71] Figure 3A−C shows that minor changes are observed in the NKP for all three proteins, for data collected at 20 °C and a series of pressures up to 3 kbar: scattering profiles are well conserved and superimposable with the corresponding nonpressurized sample. Scattering from each initial nonpressurized sample in solution was also compared to simulated scattering intensities from the corresponding crystal structures or homology models. A reasonable agreement was found between the Cryson[72] prediction algorithm and the experimental data for all three proteins under atmospheric conditions (black solid lines in Figure 3A−C).

A single peak is observed in the NKPs for both aCgn and Ova, while multiple peaks are observed for AS-IgG1. The bell-shaped curves obtained for aCgn solutions allow one to identify a peak maximum of ∼1.1 at a $qR_g \sim \sqrt{3} \approx 1.73$. This is in good agreement with structures of other globular

https://doi.org/10.1021/acs.molpharmaceut.1c00604
Mol. Pharmaceutics 2021, 18, 4415−4427

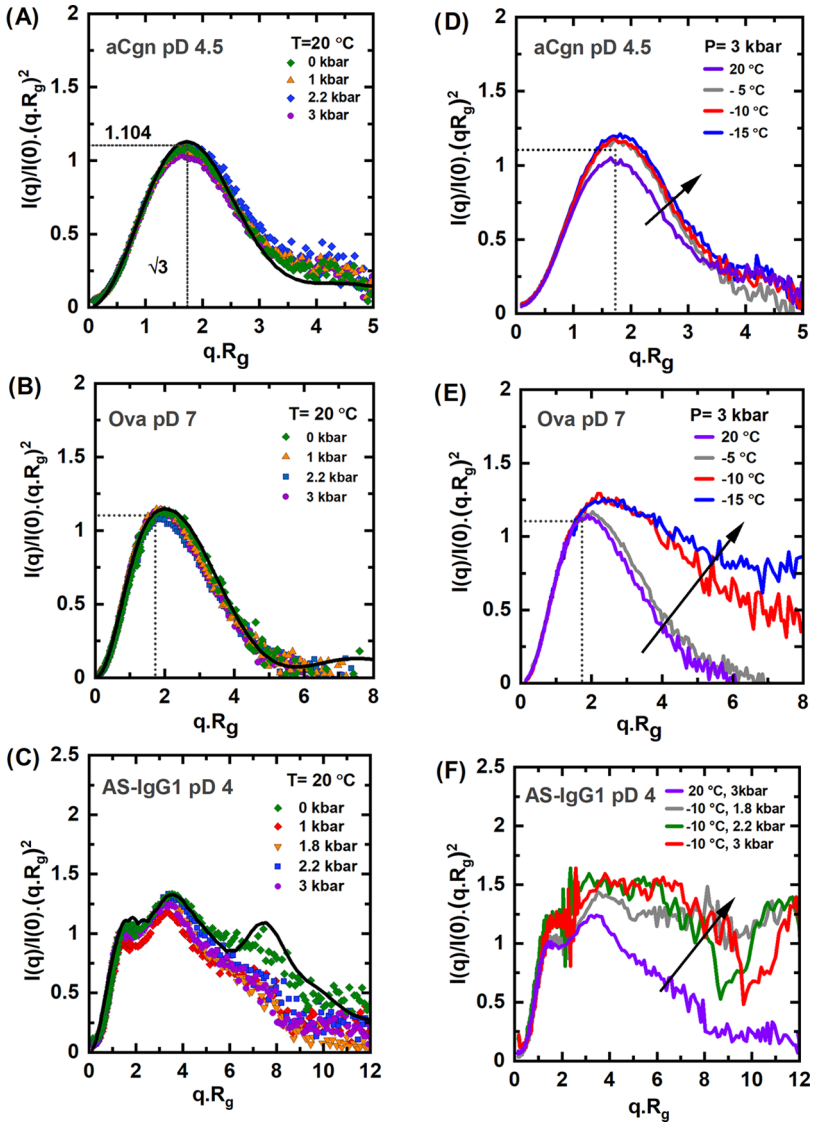

Figure 3. Normalized SANS Kratky plots for various temperature (T) conditions under high-pressure (HP) environments: (A, D) 10 mg/L aCgn in 10 mM acetate buffer pD 4.5; (B, E) 10 mg/mL Ova in 10 mM histidine buffer pD 7; (C, F) 5 mg/mL AS-IgG1 in 5 mM citrate buffer pD 4. The conditions tested are labeled for each protein solution: (1) T = 20 °C and a series of P conditions—plots (A), (B), and (C); (2) a series of low-T conditions down to −15 °C and P = 3 kbar—plots (D) and (E); and (3) series of P up to 3 kbar and T = −10 °C—plot (F). A reference curve obtained for each protein at 20 °C and 3 kbar is shown in plots (D), (E), and (F). Arrows point toward decreasing T at 3 kbar—plots (D) and (E)—or increasing P at −10 °C—plot (F). Scattering intensities were normalized to the low-q limit, and the q value was normalized to the R_g values shown in Figure 2. Black solid lines represent the best-fit curves to $I(q)$ using Cryson software[72] with PDB structure files for the respective proteins.

proteins.[73] Ova has a roughly ellipsoid shape, and this causes an increase in the NKP peak maximum position compared with aCgn (Figure 3B). The two main peaks of AS-IgG1 (qR_g ∼ 1.5 and 3.1, shown in Figure 3C) are typical of the structure of IgG1 multidomain proteins. It was demonstrated elsewhere that other MAbs have a similar profile and these peaks should match individual F_{ab} and F_c domains. It was also suggested that these peaks are related with intra/interdomain protein distance correlations.[74−76] At a higher qR_g range of ∼7.5, a third peak appears, which is likely due to the flexible hinge region.[77] This peak seems to become less intense as AS-IgG1 solutions are pressurized up to 3 kbar, and this suggests that some conformational distortion may occur at this point. Notably, the Cryson prediction for the AS-IgG1 profile (black solid line in Figure 3C) suggests that the peak observed in the high-q range (qR_g ∼ 7.5) for the nonpressurized sample is higher in intensity than that observed experimentally under a high pressure in the liquid state. In general, deviations between the simulated curves and the experimental data are not unexpected—e.g., in a crystal structure or related homology model, proteins are in a considerably different physicochemical environment.

As the temperature is lowered to −15 °C and pressure increases to 3 kbar, NKP changes are noticeable for all three proteins. Interestingly, aCgn conformational seem to be the least impacted (Figure 3D). Nevertheless, a slight increase of the aCgn NKP peak maximum value suggests some minor native structural alteration. Additional HP-SANS measurements, carried out separately, show that the aCgn globular structure is also maintained under neutral conditions (data not shown).

https://doi.org/10.1021/acs.molpharmaceut.1c00604
Mol. Pharmaceutics 2021, 18, 4415−4427

Significant conformational changes were apparent for Ova at −10 °C and 3 kbar (e.g., NKP plateaus at higher q) as Figure 3E shows. In addition, similar NKP profiles were obtained at both −10 and −15 °C and seem to be independent of the particular pressure range tested (data not shown). The results suggest a minor contribution of elevated pressure to Ova conformational state variation while cold-temperature conditions seem to have a major role (corroborated also by Figure 2B)—i.e., the protein size/structure is maintained for a fixed low-temperature condition as pressure increases up to 3 kbar. Preliminary studies were also carried out using a custom-made HP cell for SAXS, at the Cornell High Energy Synchrotron Source (CHESS). The SAXS HP cell design and corresponding protein studies under pressure environment have been described elsewhere.[78−80] The results obtained from SAXS runs show that no significant conformational changes can be detected for Ova and aCgn (prepared in the corresponding H_2O-based buffer) at a temperature range of ∼20 to −7 °C and pressures up to ∼3 kbar (data not shown). A lower-temperature range was not possible to test with the available SAXS HP cell. Nevertheless, the results are in good agreement with $R_g/R_{g,N}$ values and NKP obtained from HP-SANS profiles (Figures 2 and 3).

Conformational changes were detected for AS-IgG1 at temperatures near −5 °C as pressure was increased from 1.8 to 3 kbar (NKP is shown for −10 °C conditions, Figure 3F). This suggests that both high pressure and cold temperature can work as potential factors to trigger AS-IgG1 structural modification. Once conformational changes occur, subsequent self-association steps may be triggered due to the potential exposure of hydrophobic regions.

Pairwise distribution functions, $P(r)$, were calculated from the HP-SANS data, including estimation of the maximum dimension (D_{max}) for each protein when $P(r)$ approaches 0. When aggregation occurs, the $P(r)$ function becomes broadened and additional peaks may be observed.[81,82] For cases of extreme aggregate polydispersity, $P(r)$ may not even approach zero at large r values. The results show that only Ova samples have a significant increase in oligomeric species, reflected by a significant broadening of the $P(r)$ curve. This is observed at − 10 °C for all pressure conditions tested (Figure 4). Moreover, distinguishable multiple peaks (blue arrows in Figure 4) suggest the formation of different populations of oligomers (e.g., dimers, trimers). The results also show that the starting Ova solution (obtained under room-temperature conditions) includes a small population of dimers (green arrow in Figure 4). As Ianeselli et al. have shown, Ova molecules tend to associate to form dimers, which are stabilized by the large hydrophobic interactions.[83] The starting dimers observed at an ambient pressure and 20 °C are likely dissociated under HP conditions, as oligomeric proteins are particularly pressure-sensitive. This is demonstrated experimentally as D_{max} values decrease when pressure was increased up to 3 kbar under constant room-temperature conditions (purple curve in Figure 4).

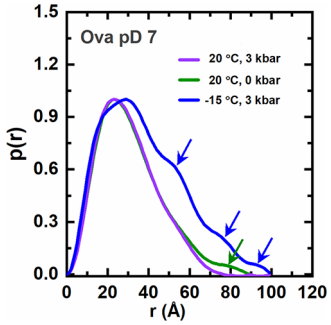

Figure 4. Pair distribution function calculated for 10 mg/mL Ova in deuterated 10 mM histidine buffer pD 7. The conditions for temperature and pressure tested are labeled in the main panel. Arrows indicate deviations to the bell-shaped curve of Ova and suggest the presence of oligomeric states.

Complementary data were obtained via FL, focused on protein conformational stability by following the unfolding process and comparing to a series of denaturant concentrations above freezing conditions and then extrapolating to sub-0 °C conditions.[50] Denaturation curves obtained via ICD were used to detect each protein unfolding transition for a given temperature of interest. This is illustrated in Figure 5A,B for aCgn and Ova, respectively: each FL profile shows that λ_{max} and $\Delta\lambda$ increase as the denaturant concentration increases. To better quantify the spectral shifts of the emission spectra, a plot of spectral center of mass (COM) as a function of denaturant concentration was used. In general, the increase of COM values is an indicator of loss of tertiary features within the protein structure. This is illustrated in Figure 5C for aCgn unfolding as the urea concentration was increased. The solid lines shown in Figure 5C are the best fit to the COM data vs urea concentration using a two-state model approximation (see the Supporting Information for details).

Figure 6A shows ΔG_{un} values plotted as a function of temperature for aCgn: the error bars of aCgn profiles represent 95% confidence intervals for the two-state model fit shown in Figure 5C; ΔG_{un} values obtained for Ova were previously reported[84] and are also plotted in Figure 6A. The solid lines in Figure 6A are calculated via the Gibbs−Helmholtz equation for aCgn and Ova and include the experimental range and the subzero regime (extrapolation region). See the Supporting Information for more details on ΔG_{un} calculation via the Gibbs−Helmholtz equation.

A T_{CD} of −19 °C (± 3) was estimated based on the extrapolation of the Gibbs−Helmholtz fit for aCgn solutions for the pH 4.5 condition. The value of T_{CD} previously reported for Ova solutions under the corresponding pH 7 condition is −17.4 °C.[84] The increasing fraction of unfolded species as temperature decreases can be estimated, within the two-state unfolding approximation, for the cold-temperature range as Figure 6B shows. ΔG_{un} values obtained near T_m for aCgn are considered in the Gibbs−Helmholtz fit for the entire temperature range. The experimental thermal scans obtained via differential scanning calorimetry (DSC) for aCgn solutions were reversible (up to 80 °C, data not shown), and this is in agreement with two-state (un)folding models. A two-state unfolding pathway was shown to be valid for aCgn solutions in prior work.[61] From a statistical standpoint, increasing the number and range of temperature conditions tested can improve ΔG_{un} predictions and extrapolations over the cold-temperature regime. However, experimental ΔG_{un} values were limited to conditions above 0 °C, and this leads to statistical uncertainties as the fits are extrapolated to the subzero conditions (Figure 6B).

Using urea as a denaturant is beneficial over guanidine hydrochloride as electrostatic protein−protein interactions are less perturbed, and this leads to improved linear extrapolation method (LEM) predictions.[85] On the other hand, guanidine

https://doi.org/10.1021/acs.molpharmaceut.1c00604
Mol. Pharmaceutics 2021, 18, 4415−4427

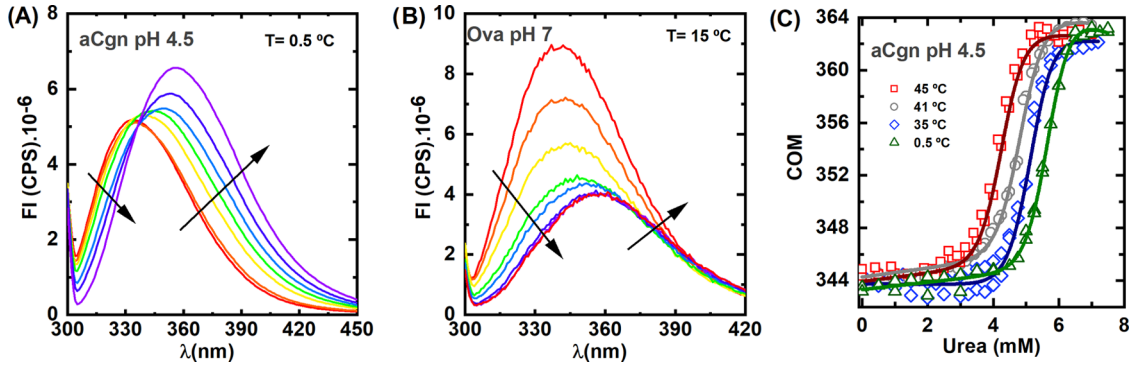

Figure 5. (A) Fluorescence intrinsic emission spectra for 0.025 mg/mL aCgn in 10 mM acetate buffer pH 4.5 at 0.5 °C for a series of urea concentration up to ∼8 M (as the arrows illustrate). (B) Fluorescence intrinsic emission spectra for 0.3 mg/mL Ova in 10 mM histidine buffer pH 7 at 15 °C for a series of urea concentration up to ∼8 M (as the arrows illustrate). (C) Fluorescence spectral center of mass (COM) for aCgn calculated as a function of urea concentration at various temperatures as labeled. Each COM unfolding profile was measured in duplicate for a given temperature. The lines are the corresponding fits to the two-state model.

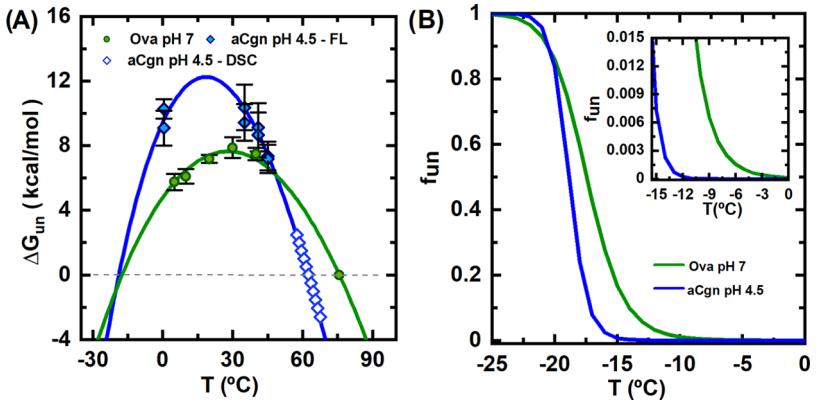

Figure 6. (A) Extrapolation of apparent ΔG_{un} values as a function of temperature to estimate a T_{CD} of −19 °C (±3) for aCgn at atmospheric pressure using the Gibbs−Helmholtz expression. ΔG_{un} values were calculated for aCgn via thermal unfolding and denaturant-induced unfolding (filled diamonds) or via differential scanning calorimetry (DSC) (empty diamonds). Error bars represent the 95% confidence intervals for ΔG_{un} obtained from the two-state model fit. Data points are the mean of two or three measurements. The extrapolation of ΔG_{un} across a range of temperatures is also shown for Ova (green symbols are experimental data obtained via chemical unfolding, and T_m value was obtained via DSC, data excerpted from ref 84); the green line shows the best fit using the Gibbs−Helmholtz expression. (B) Unfolded fraction (f_{un}) was calculated as a function of temperature for aCgn. The unfolded fraction prediction is also shown for Ova (data excerpted from ref 84).

hydrochloride is a stronger denaturant and lower concentrations are often required to induce a given unfolded state. In either case, significant extrapolation is required to obtain ΔG_{un} values at zero denaturant (e.g., the equilibrium denaturation transition for aCgn solution starts around 4 M urea). That notwithstanding, the present folding projections can be used as a surrogate for protein conformational stability under cold-temperature conditions.

Under higher-pressure conditions, intrinsic fluorescence COM profiles reveal a spectral shift of ∼1 and 5 nm for aCgn and Ova, respectively, at the lowest temperature tested of −14 °C (Figure S1, Supporting Information). This is significantly smaller in magnitude compared to that observed for fully unfolded transitions ($\Delta\lambda$ ∼ 15−20 nm) during chemical unfolding experiments (Figures S1 and 5). This was taken to indicate that the *in situ* conformational changes for Ova (Figure 3E) over the cold-temperature regime are likely to occur because the temperature is approaching T_{CD} (∼−17 °C, Figure 6A) rather than a pressure effect (Figures 3B and S1). Moreover, the sensitivity of the *in situ* SANS approach enables detection of shifts in structural conformations, the presence of unfolded or partially unfolded populations, and oligomeric states at temperatures below −10 °C.

For AS-IgG1, a different scenario is proposed. That is, the pressure range required to perturb AS-IgG1 native structures under cold environment is lower than 3 kbar (Figures 2C and 3F). Additional FL data were collected under high-pressure conditions to capture tertiary structural changes for AS-IgG1. Figure 7A/B shows illustrative HP-FL profiles for AS-IgG1 obtained over the lowest (−10 °C)/highest (50 °C) temperatures tested for a series of pressures up to 3 kbar. Note that the starting pressure for the −10 °C condition was 1.3 kbar to avoid freezing events. The corresponding COM data as a function of a given applied pressure are shown for a series of high-temperature (Figure 7C) and low-temperature (Figure 7D) conditions: $\Delta\lambda$ values of ∼8 and ∼20 nm are observed at −10 and 50 °C, respectively. Furthermore, the results show that the unfolding transition at 50 °C seems to be near complete due to a well-defined sigmoidal curve with large $\Delta\lambda$ and a sharp transition region (Figure 7C). The NKP data obtained for AS-IgG1 also suggest the presence of an unfolded state for high-temperature conditions (Figure S2, Supporting Information). In contrast, the denaturation curves obtained under sub-0 °C conditions seem to only capture the first unfolding event for AS-IgG1 (small $\Delta\lambda$ and small transition region). Unfolding intermediates (or "molten globule" states)

https://doi.org/10.1021/acs.molpharmaceut.1c00604
Mol. Pharmaceutics 2021, 18, 4415−4427

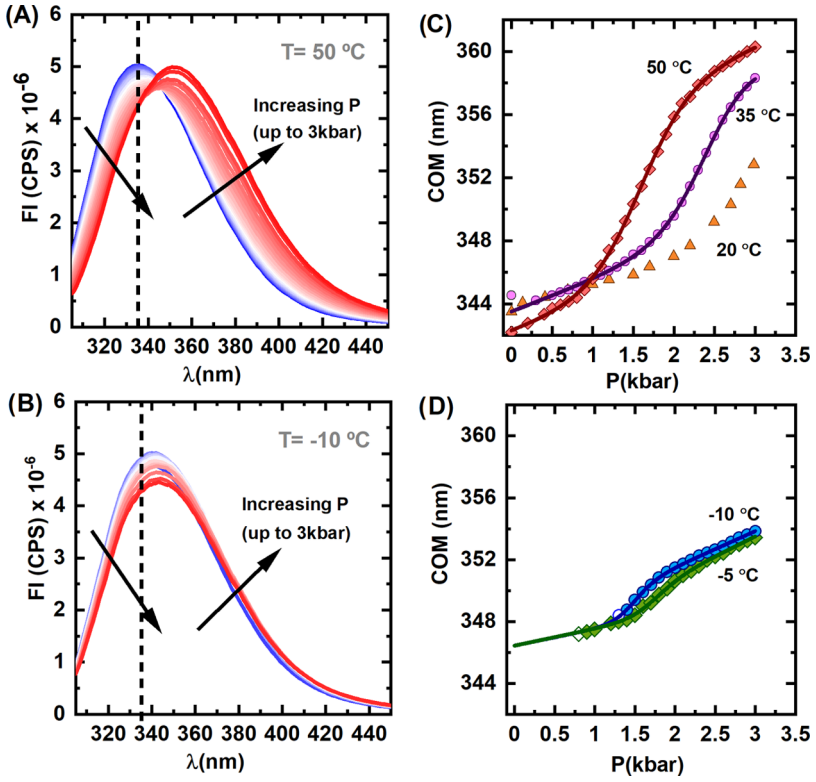

Figure 7. Intrinsic fluorescence emission spectra for AS-IgG1 0.15 mg/mL prepared in 5 mM citrate buffer pH 4, recorded as a function of increasing P (as arrows show) at (A) 50 °C and (B) −10 °C. Spectral center of mass (COM) calculated from the emission spectra as a function of increasing pressure for a series of high T (C) and low T (D) as labeled in each panel. Solid lines correspond to a two-state unfolding model fit to obtain estimates of apparent $\Delta G_{0,un}$ and $\Delta v_{0,un}$ values for each condition tested.

have been reported for several globular proteins,[10,20,21] unlike for multidomain proteins such as MAbs.[13] However, the presence of intermediate species within a typical Mab molecule has typically been tested using high temperatures or high concentrations of chemical denaturants as the stressing agent, rather than elevated pressure and/or cold temperatures.

Several studies have reported different structural protein conformations for high-pressure environments and/or cold-temperature regimes compared with high-temperature conditions. The former induces the formation of compact denatured states, whereas the latter may lead to the formation of more disordered structures.[30,42,86,87] As noted above, one may expect large deviations to the thermodynamic behavior of multidomain proteins when experiments are simply carried out *ex situ* at high temperatures, and thermodynamic parameters are obtained via extrapolated methods.

The fit parameters obtained for each FL denaturation curve (solid lines—Figure 7C,D) provide information regarding pressure-induced denaturation for AS-IgG1 (Table 1). The volumetric changes that occur via pressure unfolding (ΔV_{un}) indicate at least partly the amount of solvent excluded volume as the protein unfolds: i.e., ΔV_{un} values increased as temperature decreases, and this can be directly related to different expansivity and compressibility effects over both cold- and high-temperature regimes.[88] This effect is also pH-dependent, as preliminary data show that increasing the pH of AS-IgG1 by one unit seems to increase the half-denaturation pressure (pressure required to denature half of AS-IgG1 monomers), $P_{1/2}$, and the overall conformational resistance to unfolding (Figure S3, Supporting Information).

Table 1. Apparent Thermodynamic Parameters Associated with the Pressure Denaturation of AS-IgG1 0.15 mg/mL Prepared 5 mM Citrate Buffer pH 4 Calculated from a Folding/Unfolding Two-State Model Fit[a]

T (°C)	ΔG_{un} (kJ/mol)	ΔV_{un} (mL/mol)	$P_{1/2}$ (kbar)
50	14 (±2)	− 86 (±13)	1.59 (±0.05)
35	22 (±3)	− 89 (±13)	2.50 (±0.1)
−5	23 (±5)	− 135 (±30)	1.70 (±0.06)
−10	21 (±5)	− 144 (±37)	1.47 (±0.03)

[a]The errors shown correspond to one standard deviation of uncertainty.

It should be highlighted that pH changes can occur over the pressure−temperature conditions tested. This is relevant as pH can have a role in the conformational stability of pH-sensitive proteins. Briefly, both pressure and temperature can lead to changes in pK_a values of buffers and their respective acid dissociation equilibria. Acid−base equilibria can be shifted toward positive/negative ΔV (difference in the partial molar volumes of the neutral and the ionized species in equilibrium), according to Le Chatelier's principle.[89−92] While $\Delta V \sim 0$ mL/mol leads to pressure independence of pH, for some buffers, ΔV values can be significant (∼− 5 to −20 mL/mol).[93] However, the choice of buffers in high-pressure studies can be quite limited as even with some common examples (e.g., MES, TRIS, and imidazole) that have been reported to be quite resistant to pressure changes on pK_a values[90,94] have an increase of pH of ca. 0.1−0.3 pH units/kbar.[91] In the context of the current report, citrate buffer used to prepare the ASA-IgG1 solutions at pH 4 has a ΔV of −12.3 mL/mol for the

https://doi.org/10.1021/acs.molpharmaceut.1c00604
Mol. Pharmaceutics 2021, 18, 4415−4427

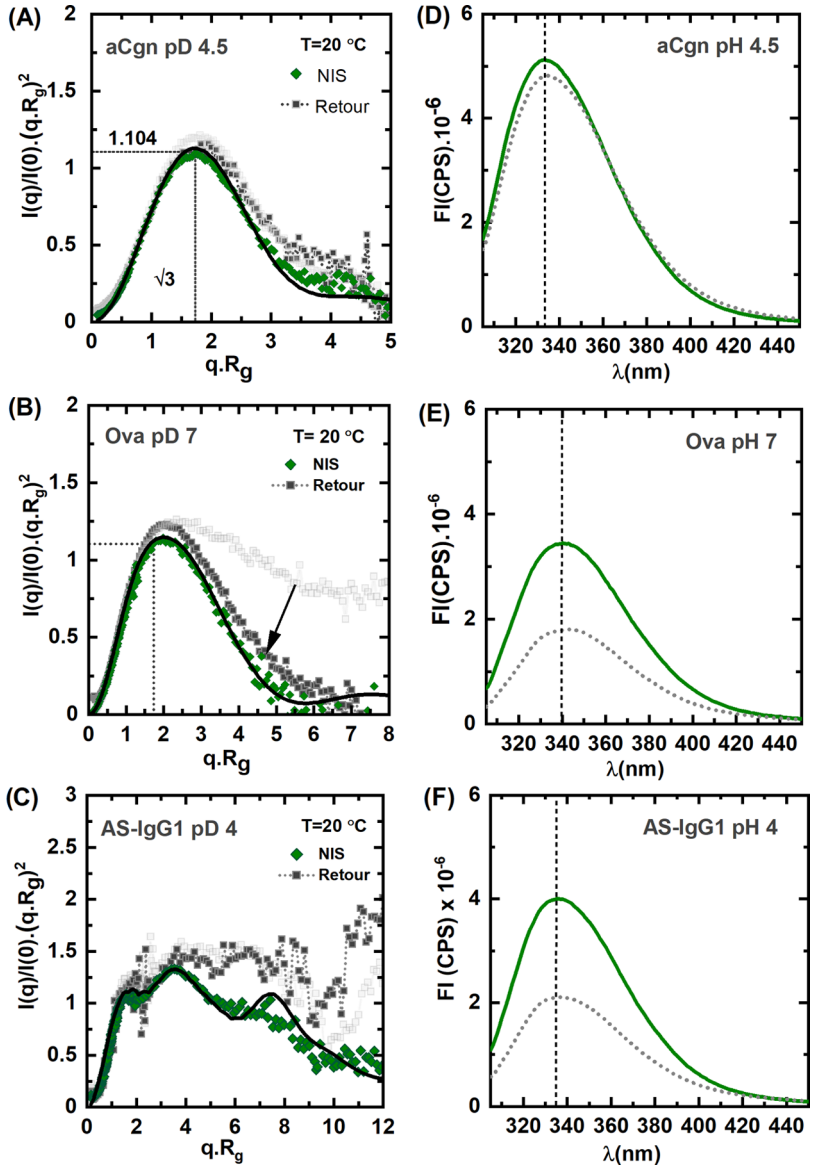

Figure 8. Normalized SANS Kratky plots (A–C) and intrinsic fluorescence profiles (D–F) for a given protein system at a temperature of 20 °C: aCgn, 10 mg/mL in 10 mM acetate buffer pD 4.5 (A) and (D); Ova 10 mg/mL in 10 mM histidine buffer pD 7 (B) and (E); AS-IgG1 5 mg/mL in 5 mM citrate buffer pD 4 (C) and (F). The conditions shown demonstrate reversibility behavior of each protein (labeled in each main panel): (1) starting nonincubated samples (NIS) that were not pressurized—green symbols (A–C)/green continuous lines (D–F); (2) reference SANS profiles obtained after a given sample is pressurized up to 3 kbar and cooled down to −15 °C (A and B) or −10 °C (C)—light gray symbols; and (3)—SANS and Fl profiles obtained after pressure and temperature stress—dark gray symbols (A–C)/dotted lines (D–F). Black solid lines represent the best-fit curves to NIS using each Protein Data Bank file and Cryson software.[72]

relevant ionizable group;[93] a decrease in pH can be expected to be up to ∼0.8 pH units for the pressure range tested here.[95] Hence, although it is not typically feasible to make a direct measurement of pH changes under those high-pressure environments, it is possible that the values of $P_{1/2}$ obtained AS-IgG1 in citrate buffer at pD 4 could be different from the ones measured (Table 1) if pH (or pD) were constant. The acetate buffer used in the aCgn solutions at pH 4.5 has a ΔV of −11.2 mL/mol[90] and an increase in pH has been reported to be approximately −0.08 units/kbar.[91]

Overall, the choice of pressure- and temperature-resistant buffers is not a straightforward task. Even the best combination of baroresistant buffers suggested by Quilan and Reinhart[91] can remain temperature-sensitive.[95] For instance, TRIS is a less pressure-sensitive buffer (ΔV = 4.3 mL/mol) but has a large dependence of temperature (0.028 ΔpH unit/°C);[95] this can still lead to higher pH changes if higher-/lower-temperature conditions are considered. As noted above, citrate buffer has a higher dependence on pressure; however, it is expected to have a lower temperature dependence over the range +25 to −30 °C.[96] This lower temperature dependence is also observed for the other buffer systems (acetate and histidine-HCl) selected for the present study.[96]

Finally, the reversibility of cold and/or pressure unfolded states was evaluated. The reversibility analysis was performed via HP-FL and HP-SANS by comparing unstressed samples with those that were stressed after they were returned to ambient temperature and pressure. Figure 8 shows the corresponding reversibility profiles at the end of each set of cold-temperature and pressure conditions. The results show

https://doi.org/10.1021/acs.molpharmaceut.1c00604
Mol. Pharmaceutics 2021, 18, 4415−4427

that NKP and FL profiles are similar and nearly superimposable for aCgn (Figure 8A,D) and Ova (Figure 8B,E) before and after P/T stress, which suggests that the protein structure was recovered close to their respective native (unstressed) conformations.

In contrast, conformational changes were not reversed for AS-IgG1 solutions. The plateau observed in the NKP profiles for cold-temperature conditions is maintained (gray symbols in Figure 8C), and FL profiles also show a significant decrease in fluorescence intensity (Figure 8F). This suggests that AS-IgG1 adopts an irreversible non-native conformation after cold and pressure stress. Although it is well known that globular proteins can reversibly fold when subjected to pressures up to 7 kbar (under room-temperature conditions),[42] limited work has addressed the specific conformational states of MAbs under high-pressure conditions. Some have proposed that irreversible changes are expected to occur at lower pressures than those required for other globular proteins. For instance, König et al.[41] have shown that irreversible structural changes occur at ∼5 kbar for an IgG under room-temperature conditions, but the *Y*-shape conformation is still maintained. In other reports, Howlett and co-workers[97] have shown that a bovine IgG structure is sensitive to a pressure range of 2−4 kbar and this was further related with observed aggregation events.

It was out of the scope of the present work to provide an in-depth thermodynamic analysis of complete unfolding curves, as that would require higher pressures than were accessible here to test fully unfolded states. Instead, the present work focused on high-pressure and cold-temperature ranges needed to initially perturb the relevant structures for globular and multidomain proteins. This can potentially provide insights into the influence of protein thermodynamic stability under cold-temperature conditions. Rosa et al. proposed that the pressure effect on a model globular protein (bovine hemoglobin) in the cold-temperature regime was negligible by performing isochoric experiments (*ex situ* approach).[80] Both globular proteins tested here have shown to be resistant to pressures up to 3 kbar under low-temperature conditions, which is higher than the pressure range associated with isochoric methods (pressure increases up to ∼1.5 kbar at −15 °C). Instead, Ova structural changes and the first protein−protein assembly steps detected via *in situ* HP-SANS below −10 °C are assumed to be induced solely by cold-temperature conditions. This is in good agreement with the high aggregation rates obtained for identical Ova solutions stored under isochoric conditions below −10 °C.[84] AS-IgG1, however, showed a combination of sensitivity to cold temperatures and elevated pressures, illustrating that assumptions for MAbs concerning the sensitivity to cold temperatures and/or high pressures that are based on globular proteins under the same solution conditions may not hold generally (e.g., may depend on the solution conditions), and globular proteins may not be good model examples for therapeutic proteins such as MAbs. This also highlights how unfolding and association events can be difficult to deconvolute when only an *ex situ* approach is considered.

Finally, *ex situ* approaches are usually followed by quenching steps, which are intended to arrest a given structural/aggregation state, but those changes are not static and can be potentially reversed if the medium conditions change. It is also possible that the T_{CD} of proteins could be shifted toward lower values under high-pressure conditions, and this is proposed here for AS-IgG1 under acidic conditions. As an alternative, the *in situ* methods described in this work are a promising approach to evaluate protein conformational/structural stability providing a more comprehensive framework to understand potential pathways for protein non-native aggregation events.

4. SUMMARY AND CONCLUSIONS

Protein conformational stability evaluation by *in situ* approaches under cold conditions (sub-0 °C) is attractive as it provides capabilities that are not typically accessible with mainstream analytical techniques, and there are well-known issues with using high-temperature stability data for interpreting or extrapolating to cold-temperature conditions. To this end, SANS and FL techniques were combined with high-pressure experimental configurations to access sub-0 °C conditions and assess conformational changes and unfolding for three example systems ranging from small globular proteins to a large multidomain monoclonal antibody. The results illustrate that pressures below 3 kbar are generally not enough to significantly unfold aCgn down to temperatures of −15 °C. Additionally, structural changes observed for Ova via HP-SANS seem to be induced by the lower temperatures rather than the effects of high pressure. It is likely that this reflects the proximity to the T_{CD} value for Ova based on cold-induced unfolding extrapolation methods. However, direct evidence of intermediary unfolded states and the formation of oligomeric species was observed at −10 °C, and this is outside the prediction capabilities of standard *ex situ* methods. Denaturation and conformational changes due to the combined effect of subzero temperature and elevated pressure were observed for AS-IgG1 at $P \sim 2$ kbar and T of −5 °C. Additional thermodynamic analysis of HP-FL data suggests that AS-IgG1 has a larger ΔV_{un} if compared with the two globular proteins studied here. AS-IgG1 volumetric changes are suggested to be temperature-dependent, and conformational states seem to be different in the cold-temperature vs high-temperature regimes. The present work illustrates *in situ* HP-SANS and HP-FL methods that have the potential to improve protein stability assessments and model predictions based on structural changes and unfolding thermodynamics without relying on high-temperature approaches.

■ ASSOCIATED CONTENT

Supporting Information

The Supporting Information is available free of charge at https://pubs.acs.org/doi/10.1021/acs.molpharmaceut.1c00604.

Additional experimental details for fluorescence data analysis, neutron scattering, and additional illustrative data from neutron scattering (PDF)

■ AUTHOR INFORMATION

Corresponding Author

Christopher J. Roberts − *Department of Chemical and Biomolecular Engineering, University of Delaware, Newark, Delaware 19713, United States;* orcid.org/0000-0001-9978-2767; Phone: 302-831-0838; Email: cjr@udel.edu; Fax: 302-831-1048

Authors

Diana C. Gomes − *Centro de Química Estrutural, Departamento de Engenharia Química, Instituto Superior*

https://doi.org/10.1021/acs.molpharmaceut.1c00604
Mol. Pharmaceutics 2021, 18, 4415−4427

Técnico, Universidade de Lisboa, 1049-001 Lisboa, Portugal; Department of Chemical and Biomolecular Engineering, University of Delaware, Newark, Delaware 19713, United States

Susana C. M. Teixeira − *Department of Chemical and Biomolecular Engineering, University of Delaware, Newark, Delaware 19713, United States; NIST Center for Neutron Research, National Institute of Standards and Technology, Gaithersburg, Maryland 20899, United States*

Juscelino B. Leão − *NIST Center for Neutron Research, National Institute of Standards and Technology, Gaithersburg, Maryland 20899, United States*

Vladimir I. Razinkov − *Drug Product Development, Amgen Inc., Thousand Oaks, California 91320, United States*

Wei Qi − *Drug Product Development, Amgen Inc., Thousand Oaks, California 91320, United States*

Miguel A. Rodrigues − *Centro de Química Estrutural, Departamento de Engenharia Química, Instituto Superior Técnico, Universidade de Lisboa, 1049-001 Lisboa, Portugal*

Complete contact information is available at: https://pubs.acs.org/10.1021/acs.molpharmaceut.1c00604

Notes

Certain commercial equipment, instruments, and suppliers are identified to foster understanding. This does not imply recommendation or endorsement by the National Institute of Standards and Technology, nor does it imply that the materials or equipment identified are necessarily the best available for the purpose.

The authors declare no competing financial interest.

■ ACKNOWLEDGMENTS

This manuscript was prepared under cooperative agreement 70NANB12H239 and 370NANB17H302 from NIST, U.S. Department of Commerce. The authors acknowledge the support of the National Institute of Standards and Technology, U.S. Department of Commerce, in providing the neutron research facilities used in this work. The statements, findings, conclusions, and recommendations are those of the authors and do not necessarily reflect the view of NIST or the U.S. Department of Commerce. D.C.G., S.C.M.T., and C.J.R. gratefully acknowledge funding from NIST.

■ REFERENCES

(1) Shalaev, E.; Soper, A.; Zeitler, J. A.; Ohtake, S.; Roberts, C. J.; Pikal, M. J.; Wu, K.; Boldyreva, E. Freezing of Aqueous Solutions and Chemical Stability of Amorphous Pharmaceuticals: Water Clusters Hypothesis. *J. Pharm. Sci.* **2019**, *108*, 36−49.

(2) Brummitt, R. K.; Nesta, D. P.; Roberts, C. J. Predicting Accelerated Aggregation Rates for Monoclonal Antibody Formulations, and Challenges for Low-Temperature Predictions. *J. Pharm. Sci.* **2011**, *100*, 4234−4243.

(3) Rosa, M.; Lopes, C.; Melo, E. P.; Singh, S. K.; Geraldes, V.; Rodrigues, M. A. Measuring and Modeling Hemoglobin Aggregation below the Freezing Temperature. *J. Phys. Chem. B* **2013**, *117*, 8939−8946.

(4) Sanfelice, D.; Temussi, P. A. Cold Denaturation as a Tool to Measure Protein Stability. *Biophys. Chem.* **2016**, *208*, 4−8.

(5) Rizzo, J. M.; Shi, S.; Li, Y.; Semple, A.; Esposito, J. J.; Yu, S.; Richardson, D.; Antochshuk, V.; Shameem, M. Application of a High-Throughput Relative Chemical Stability Assay to Screen Therapeutic Protein Formulations by Assessment of Conformational Stability and Correlation to Aggregation Propensity. *J. Pharm. Sci.* **2015**, *104*, 1632−1640.

(6) Chi, E. Y.; Krishnan, S.; Kendrick, B. S.; Chang, B. S.; Carpenter, J. F.; Randolph, T. W. Roles of Conformational Stability and Colloidal Stability in the Aggregation of Recombinant Human Granulocyte Colony-Stimulating Factor. *Protein Sci.* **2003**, *12*, 903−913.

(7) Wang, X.; Kumar, S.; Buck, P. M.; Singh, S. K. Impact of Deglycosylation and Thermal Stress on Conformational Stability of a Full Length Murine IgG2a Monoclonal Antibody: Observations from Molecular Dynamics Simulations. *Proteins* **2013**, *81*, 443−460.

(8) Berner, C.; Menzen, T.; Winter, G.; Svilenov, H. L. Combining Unfolding Reversibility Studies and Molecular Dynamics Simulations to Select Aggregation-Resistant Antibodies. *Mol. Pharmaceutics* **2021**, *18*, 2242−2253.

(9) Gentiluomo, L.; Svilenov, H. L.; Augustijn, D.; El Bialy, I.; Greco, M. L.; Kulakova, A.; Indrakumar, S.; Mahapatra, S.; Morales, M. M.; Pohl, C.; et al. Advancing Therapeutic Protein Discovery and Development through Comprehensive Computational and Biophysical Characterization. *Mol. Pharmaceutics* **2020**, *17*, 426−440.

(10) Mizuguchi, M.; Hashimoto, D.; Sakurai, M.; Nitta, K. Cold Denaturation of α-Lactalbumin. *Proteins: Struct., Funct., Genet.* **2000**, *38*, 407−413.

(11) Luan, B.; Shan, B.; Baiz, C.; Tokmakoff, A.; Raleigh, D. P. Cooperative Cold Denaturation: The Case of the C-Terminal Domain of Ribosomal Protein L9. *Biochemistry* **2013**, *52*, 2402−2409.

(12) Pastore, A.; Martin, S. R.; Politou, A.; Kondapalli, K. C.; Stemmler, T.; Temussi, P. A. Unbiased Cold Denaturation: Low- and High-Temperature Unfolding of Yeast Frataxin under Physiological Conditions. *J. Am. Chem. Soc.* **2007**, *129*, 5374−5375.

(13) Lazar, K. L.; Patapoff, T. W.; Sharma, V. K. Cold Denaturation of Monoclonal Antibodies. *mAbs* **2010**, *2*, 42−52.

(14) Griko, Y. V.; Privalov, P. L. Calorimetric Study of the Heat and Cold Denaturation of β-Lactoglobulin. *Biochemistry* **1992**, *31*, 8810−8815.

(15) Singh, S. K.; Kolhe, P.; Mehta, A. P.; Chico, S. C.; Lary, A. L.; Huang, M. Frozen State Storage Instability of a Monoclonal Antibody: Aggregation as a Consequence of Trehalose Crystallization and Protein Unfolding. *Pharm. Res.* **2011**, *28*, 873−885.

(16) Shivu, B.; Seshadri, S.; Li, J.; Oberg, K. A.; Uversky, V. N.; Fink, A. L. A. L.; Lendel, C.; Bolognesi, B.; Wahlström, A.; Dobson, C. M.; et al. Protein Aggregation: Folding Aggregates, Inclusion Bodies and Amyloid. *Biochemistry* **2013**, *3*, 2555−2561.

(17) Rowe, J. B.; Flynn, R. P.; Wooten, H. R.; Noufer, H. A.; Cancel, R. A.; Zhang, J.; Subramony, J. A.; Pechenov, S.; Wang, Y. Submicron Aggregation of Chemically Denatured Monoclonal Antibody. *Mol. Pharmaceutics* **2018**, *15*, 4710−4721.

(18) Matysiak, S.; Debenedetti, P. G.; Rossky, P. J. Role of Hydrophobic Hydration in Protein Stability: A 3D Water-Explicit Protein Model Exhibiting Cold and Heat Denaturation. *J. Phys. Chem. B* **2012**, *116*, 8095−8104.

(19) Fu, H.; Grimsley, G.; Scholtz, J. M.; Pace, C. N. Increasing Protein Stability: Importance of DeltaC(p) and the Denatured State. *Protein Sci.* **2010**, *19*, 1044−1052.

(20) Vidugiris, G. J. A.; Royer, C. A. Determination of the Volume Changes for Pressure-Induced Transitions of Apomyoglobin between the Native, Molten Globule, and Unfolded States. *Biophys. J.* **1998**, *75*, 463−470.

(21) Kitahara, R.; Simorellis, A. K.; Hata, K.; Maeno, A.; Yokoyama, S.; Koide, S.; Akasaka, K. A Delicate Interplay of Structure, Dynamics, and Thermodynamics for Function: A High Pressure NMR Study of Outer Surface Protein A. *Biophys. J.* **2012**, *102*, 916−926.

(22) Sosnick, T. R.; Trewhella, J. Denatured States of Ribonuclease A Have Compact Dimensions and Residual Secondary Structure. *Biochemistry* **1992**, *31*, 8329−8335.

(23) Chalikian, T. V.; Völker, J.; Anafi, D.; Breslauer, K. J. The Native and the Heat-Induced Denatured States of α-Chymotrypsinogen A: Thermodynamic and Spectroscopic Studies. *J. Mol. Biol.* **1997**, *274*, 237−252.

(24) Herberhold, H.; Winter, R. Temperature- and Pressure-Induced Unfolding and Refolding of Ubiquitin: A Static and Kinetic

Fourier Transform Infrared Spectroscopy Study. *Biochemistry* **2002**, *41*, 2396−2401.
(25) Bhatnagar, B. S.; Bogner, R. H.; Pikal, M. J. Protein Stability during Freezing: Separation of Stresses and Mechanisms of Protein Stabilization. *Pharm. Dev. Technol.* **2007**, *12*, 505−523.
(26) Rathore, N.; Rajan, R. S. Current Perspectives on Stability of Protein Drug Products during Formulation, Fill and Finish Operations. *Biotechnol. Prog.* **2008**, *24*, 504−514.
(27) Rodrigues, M. A.; Miller, M. A.; Glass, M. A.; Singh, S. K.; Johnston, K. P. Effect of Freezing Rate and Dendritic Ice Formation on Concentration Profiles of Proteins Frozen in Cylindrical Vessels. *J. Pharm. Sci.* **2011**, *100*, 1316−1329.
(28) Rodrigues, M. A.; Balzan, G.; Rosa, M.; Gomes, D.; de Azevedo, E. G.; Singh, S. K.; Matos, H. A.; Geraldes, V. The Importance of Heat Flow Direction for Reproducible and Homogeneous Freezing of Bulk Protein Solutions. *Biotechnol. Prog.* **2013**, *29*, 1212−1221.
(29) Geraldes, V.; Gomes, D. C.; Rego, P.; Fegley, D.; Rodrigues, M. A. A New Perspective on Scale-Down Strategies for Freezing of Biopharmaceutics by Means of Computational Fluid Dynamics. *J. Pharm. Sci.* **2020**, *109*, 1978−1989.
(30) Roche, J.; Royer, C. A.; Roumestand, C. Monitoring Protein Folding through High Pressure NMR Spectroscopy. *Prog. Nucl. Magn. Reson. Spectrosc.* **2017**, *102*−*103*, 15−31.
(31) Kunugi, S.; Tanaka, N. Cold Denaturation of Proteins under High Pressure. *Biochim. Biophys. Acta, Protein Struct. Mol. Enzymol.* **2002**, *1595*, 329−344.
(32) Seemann, H.; Winter, R.; Royer, C. A. Volume, Expansivity and Isothermal Compressibility Changes Associated with Temperature and Pressure Unfolding of Staphylococcal Nuclease. *J. Mol. Biol.* **2001**, *307*, 1091−1102.
(33) Meersman, F.; Dobson, C. M. Probing the Pressure-Temperature Stability of Amyloid Fibrils Provides New Insights into Their Molecular Properties. *Biochim. Biophys. Acta, Proteins Proteomics* **2006**, *1764*, 452−460.
(34) Matthews, B. W. Proteins under Pressure. *Proc. Natl. Acad. Sci. U.S.A.* **2012**, *109*, 6792−6793.
(35) John, R. J. S.; Carpenter, J. F.; Randolph, T. W. High-Pressure Refolding of Disulfide-Cross-Linked Lysozyme Aggregates: Thermodynamics and Optimization. *Biotechnol. Prog.* **2002**, *18*, 565−571.
(36) Kim, Y. S.; Randolph, T. W.; Seefeldt, M. B.; Carpenter, J. F. High-Pressure Studies on Protein Aggregates and Amyloid Fibrils. *Methods Enzymol.* **2006**, *413*, 237−253.
(37) Frye, K. J.; Royer, C. A. Probing the Contribution of Internal Cavities to the Volume Change of Protein Unfolding under Pressure. *Protein Sci.* **1998**, *7*, 2217−2222.
(38) Royer, C. A. Revisiting Volume Changes in Pressure-Induced Protein Unfolding. *Biochim. Biophys. Acta, Protein Struct. Mol. Enzymol.* **2002**, *1595*, 201−209.
(39) Kuwata, K.; Li, H.; Yamada, H.; Batt, C. A.; Goto, Y.; Akasaka, K. High Pressure NMR Reveals a Variety of Fluctuating Conformers in β-Lactoglobulin. *J. Mol. Biol.* **2001**, *305*, 1073−1083.
(40) Kitahara, R.; Akasaka, K. Close Identity of a Pressure-Stabilized Intermediate with a Kinetic Intermediate in Protein Folding. *Proc. Natl. Acad. Sci. U.S.A.* **2003**, *100*, 3167−3172.
(41) König, N.; Paulus, M.; Julius, K.; Schulze, J.; Voetz, M.; Tolan, M. Antibodies under Pressure: A Small-Angle X-Ray Scattering Study of Immunoglobulin G under High Hydrostatic Pressure. *Biophys. Chem.* **2017**, *231*, 45−49.
(42) Winter, R.; Dzwolak, W.; Wolynes, P. G.; Dobson, C. M.; Saykally, R. J. Exploring the Temperature-Pressure Configurational Landscape of Biomolecules: From Lipid Membranes to Proteins. *Philos. Trans. R. Soc., A* **2005**, *363*, 537−563.
(43) Brandts, J. F.; Oliveira, R. J.; Westort, C. Thermodynamics of Protein Denaturation. Effect of Pressure on the Denaturation of Ribonuclease A. *Biochemistry* **1970**, *9*, 1038−1047.
(44) Hawley, S. A. Reversible Pressure-Temperature Denaturation of Chymotrypsinogen. *Biochemistry* **1971**, *10*, 2436−2442.
(45) Maeno, A.; Matsuo, H.; Akasaka, K. The Pressure-Temperature Phase Diagram of Hen Lysozyme at Low PH. *Biophysics* **2009**, *5*, 1−9.
(46) Gomes, D.; Kalman, R. K.; Pagels, R. K.; Rodrigues, M. A.; Roberts, C. J. Parallel Chromatography and in Situ Scattering to Interrogate Competing Protein Aggregation Pathways. *Protein Sci.* **2018**, *27*, 1325−1333.
(47) Li, Y.; Ogunnaike, B. A.; Roberts, C. J. Multi-Variate Approach to Global Protein Aggregation Behavior and Kinetics: Effects of PH, NaCl, and Temperature for α-Chymotrypsinogen A. *J. Pharm. Sci.* **2010**, *99*, 645−662.
(48) Gibbs, S. J.; Chu, A. S.; Lightfoot, E. N.; Root, T. W. Ovalbumin Diffusion at Low Ionic Strength. *J. Phys. Chem. A* **1991**, *95*, 467−471.
(49) Kim, N.; Remmele, R. L.; Liu, D.; Razinkov, V. I.; Fernandez, E. J.; Roberts, C. J. Aggregation of Anti-Streptavidin Immunoglobulin Gamma-1 Involves Fab Unfolding and Competing Growth Pathways Mediated by PH and Salt Concentration. *Biophys. Chem.* **2013**, *172*, 26−36.
(50) Scholtz, J. M.; Grimsley, G. R.; Pace, C. N. Solvent Denaturation of Proteins and Interpretations of the m Value. *Methods Enzymol.* **2009**, *466*, 549−565.
(51) Covington, A. K.; Paabo, M. M.; Robinson, R. A.; Bates, R. G. Use of the Glass Electrode in Deuterium Oxide and the Relation between the Standardized pD (paD) Scale and the Operational pH in Heavy Water. *Anal. Chem.* **1968**, *40*, 700−706.
(52) Rubinson, K. A. Practical Corrections for p(H,D) Measurements in Mixed H2O/D2O Biological Buffers. *Anal. Methods* **2017**, *9*, 2744−2750.
(53) Krężel, A.; Bal, W. A Formula for Correlating PKa Values Determined in D 2O and H2O. *J. Inorg. Biochem.* **2004**, *98*, 161−166.
(54) High-Pressure Cell System, 2021. http://www.iss.com/fluorescence/components/hpcell_system.html.
(55) Teixeira, S. C. M.; Leao, J. B.; Gagnon, C.; McHugh, M. A. High Pressure Cell for Bio-SANS Studies under Sub-Zero Temperatures or Heat Denaturing Conditions. *J. Neutron Res.* **2018**, *20*, 13−23.
(56) Pistorius, C. W. F. T.; Rapoport, E.; Clark, J. B. Phase Diagrams of H22O and D2O at High Pressures. *J. Chem. Phys.* **1968**, *48*, 5509−5514.
(57) Kline, S. R. Reduction and Analysis of SANS and USANS Data Using IGOR Pro. *J. Appl. Crystallogr.* **2006**, *39*, 895−900.
(58) Shiao, D. F.; Lumry, R.; Fahey, J.; Shiao, D. F. Studies of the Chymotrypsinogen Family of Proteins.XI.Heat-Capacity Changes Accompanying Reversible Thermal Unfolding of Proteins. *J. Am. Chem. Soc.* **1971**, *93*, 2024−2035.
(59) Jackson, W. M.; Brandts, J. F. Thermodynamics of Protein Denaturation. A Calorimetric Study of the Reversible Denaturation of Chymotrypsinogen and Conclusions Regarding the Accuracy of the Two-State Approximation. *Biochemistry* **1970**, *9*, 2294−2301.
(60) Brandts, J. F. The Thermodynamics of Protein Denaturation. I. The Denaturation of Chymotrypsinogen. *J. Am. Chem. Soc.* **1964**, *86*, 4291−4301.
(61) Andrews, J. M.; Roberts, C. J. Non-Native Aggregation of α-Chymotrypsinogen Occurs through Nucleation and Growth with Competing Nucleus Sizes and Negative Activation Energies. *Biochemistry* **2007**, *46*, 7558−7571.
(62) Kawachi, Y.; Kameyama, R.; Handa, A.; Takahashi, N.; Tanaka, N. Role of the N-Terminal Amphiphilic Region of Ovalbumin during Heat-Induced Aggregation and Gelation. *J. Agric. Food Chem.* **2013**, *61*, 8668−8675.
(63) Tani, F.; Shirai, N.; Onishi, T.; Venelle, F.; Yasumoto, K.; Doi, E. Temperature Control for Kinetic Refolding of Heat-Denatured Ovalbumin. *Protein Sci.* **1997**, *6*, 1491−1502.
(64) Tatsumi, E.; Yoshimatsu, D.; Hirose, M. Conformational State of Disulfide-Reduced Ovalbumin at Acidic PH. *Biosci., Biotechnol., Biochem.* **1999**, *63*, 1285−1290.
(65) Nemoto, N.; Koike, A.; Osaki, K.; Koseki, T.; Doi, E. Dynamic Light Scattering of Aqueous Solutions of Linear Aggregates Induced

https://doi.org/10.1021/acs.molpharmaceut.1c00604
Mol. Pharmaceutics 2021, 18, 4415−4427

by Thermal Denaturation of Ovalbumin. *Biopolymers* **1993**, *33*, 551−559.
(66) Broersen, K.; Weijers, M.; de Groot, J.; Hamer, R. J.; de Jongh, H. H. J. Effect of Protein Charge on the Generation of Aggregation-Prone Conformers. *Biomacromolecules* **2007**, *8*, 1648−1656.
(67) Barnett, G. V.; Razinkov, V. I.; Kerwin, B. A.; Hillsley, A.; Roberts, C. J. Acetate- and Citrate-Specific Ion Effects on Unfolding and Temperature-Dependent Aggregation Rates of Anti-Streptavidin IgG1. *J. Pharm. Sci.* **2016**, *105*, 1066−1073.
(68) Barnett, G. V.; Razinkov, V. I.; Kerwin, B. A.; Laue, T. M.; Woodka, A. H.; Butler, P. D.; Perevozchikova, T.; Roberts, C. J. Specific-Ion Effects on the Aggregation Mechanisms and Protein-Protein Interactions for Anti-Streptavidin Immunoglobulin Gamma-1. *J. Phys. Chem. B* **2015**, *119*, 5793−5804.
(69) Brummitt, R. K.; Nesta, D. P.; Chang, L.; Chase, S. F.; Laue, T. M.; Roberts, C. J. Nonnative Aggregation of an IgG1 Antibody in Acidic Conditions: Part 1. Unfolding, Colloidal Interactions, and Formation of High-Molecular-Weight Aggregates. *J. Pharm. Sci.* **2011**, *100*, 2087−2103.
(70) Gibrat, G.; Hoa, G. H. B.; Craescu, C. T.; Assairi, L.; Blouquit, Y.; Annighöfer, B.; May, R. P.; Bellissent-Funel, M. C. High-Pressure SANS and Fluorescence Unfolding Study of Calmodulin. *Biochim. Biophys. Acta, Proteins Proteomics* **2014**, *1844*, 1560−1568.
(71) Rambo, R. P.; Tainer, J. A. Characterizing Flexible and Intrinsically Unstructured Biological Macromolecules by SAS Using the Porod-Debye Law. *Biopolymers* **2011**, *95*, 559−571.
(72) Svergun, D.; Barberato, C.; Koch, M. H. CRYSOL—A Program to Evaluate X-Ray Solution Scattering of Biological Macromolecules from Atomic Coordinates. *J. Appl. Crystallogr.* **1995**, *28*, 768−773.
(73) Receveur-Brechot, V.; Durand, D. How Random Are Intrinsically Disordered Proteins? A Small Angle Scattering Perspective. *Curr. Protein Pept. Sci.* **2012**, *13*, 55−75.
(74) Castellanos, M. M.; McAuley, A.; Curtis, J. E. Investigating Structure and Dynamics of Proteins in Amorphous Phases Using Neutron Scattering. *Comput. Struct. Biotechnol. J.* **2017**, *15*, 117−130.
(75) Castellanos, M. M.; Mattison, K.; Krueger, S.; Curtis, J. E. Characterization of the NISTmAb Reference Material Using Small-Angle Scattering and Molecular Simulation: Part II: Concentrated Protein Solutions. *Anal. Bioanal. Chem.* **2018**, *410*, 2141−2159.
(76) Castellanos, M. M.; Howell, S. C.; Gallagher, D. T.; Curtis, J. E. Characterization of the NISTmAb Reference Material Using Small-Angle Scattering and Molecular Simulation: Part I: Dilute Protein Solutions. *Anal. Bioanal. Chem.* **2018**, *410*, 2141−2159.
(77) Rambo, R. P.; Tainer, J. A. Accurate Assessment of Mass, Models and Resolution by Small-Angle Scattering. *Nature* **2013**, *496*, 477−481.
(78) Ando, N.; Chenevier, P.; Novak, M.; Tate, M. W.; Gruner, S. M. High Hydrostatic Pressure Small-Angle X-Ray Scattering Cell for Protein Solution Studies Featuring Diamond Windows and Disposable Sample Cells. *J. Appl. Crystallogr.* **2008**, *41*, 167−175.
(79) Ando, N.; Barstow, B. High Hydrostatic Pressure Effect on Proteins: Fluorescence Studies. In *Encyclopedia of Analytical Chemistry*; John Wiley & Sons, Ltd., 2012.
(80) Rai, D. K.; Gillilan, R. E.; Huang, Q.; Miller, R.; Ting, E.; Lazarev, A.; Tate, M. W.; Gruner, S. M. High-Pressure Small-Angle X-Ray Scattering Cell for Biological Solutions and Soft Materials. *J. Appl. Crystallogr.* **2021**, *54*, 111−122.
(81) Molodenskiy, D.; Shirshin, E.; Tikhonova, T.; Gruzinov, A.; Peters, G.; Spinozzi, F. Thermally Induced Conformational Changes and Protein-Protein Interactions of Bovine Serum Albumin in Aqueous Solution under Different PH and Ionic Strengths as Revealed by SAXS Measurements. *Phys. Chem. Chem. Phys.* **2017**, *19*, 17143−17155.
(82) Reščič, J.; Vlachy, V.; Jamnik, A.; Glatter, O. Osmotic Pressure, Small-Angle X-Ray, and Dynamic Light Scattering Studies of Human Serum Albumin in Aqueous Solutions. *J. Colloid Interface Sci.* **2001**, *239*, 49−57.
(83) Ianeselli, L.; Zhang, F.; Skoda, M. W. A.; Jacobs, R. M. J.; Martin, R. A.; Callow, S.; Prévost, S.; Schreiber, F. Protein-Protein Interactions in Ovalbumin Solutions Studied by Small-Angle Scattering: Effect of Ionic Strength and the Chemical Nature of Cations. *J. Phys. Chem. B* **2010**, *114*, 3776−3783.
(84) Rosa, M. Development of Technology for Cryopreservation and Formulation of Therapeutic Proteins. Ph.D. Dissertation, 2016.
(85) Schellman, J. A.; Gassner, N. C. The Enthalpy of Transfer of Unfolded Proteins into Solutions of Urea and Guanidinium Chloride. *Biophys. Chem.* **1996**, *59*, 259−275.
(86) Griko YuV; Kutyshenko, V. P. Differences in the Processes of Beta-Lactoglobulin Cold and Heat Denaturations. *Biophys. J.* **1994**, *67*, 356−363.
(87) Meersman, F.; Dobson, C. M.; Heremans, K. Protein Unfolding, Amyloid Fibril Formation and Configurational Energy Landscapes under High Pressure Conditions. *Chem. Soc. Rev.* **2006**, *35*, 908−917.
(88) Dellarole, M.; Caro, J. A.; Roche, J.; Fossat, M.; Barthe, P.; García-Moreno, E. B.; Royer, C. A.; Roumestand, C. Evolutionarily Conserved Pattern of Interactions in a Protein Revealed by Local Thermal Expansion Properties. *J. Am. Chem. Soc.* **2015**, *137*, 9354−9362.
(89) Gervais, P. A Simple Method for Measuring the PH of Acid Solutions under High Pressure. *J. Phys. Chem. A* **1999**, *103*, 1785−1789.
(90) Teixeira, S. C. M. High-Pressure Small-Angle Neutron Scattering for Food Studies. *Curr. Opin. Colloid Interface Sci.* **2019**, *42*, 99−109.
(91) Quinlan, R. J.; Reinhart, G. D. Baroresistant Buffer Mixtures for Biochemical Analyses. *Anal. Biochem.* **2005**, *341*, 69−76.
(92) Min, S. K.; Chaminda, P. S.; Sastry, S. K. In Situ Measurement of Reaction Volume and Calculation of Ph of Weak Acid Buffer Solutions under High Pressure. *J. Phys. Chem. B* **2011**, *115*, 6564−6571.
(93) Kitamura, Y.; Itoh, T. Reaction Volume of Protonic Ionization for Buffering Agents. Prediction of Pressure Dependence of PH and POH. *J. Solution Chem.* **1987**, *16*, 715−725.
(94) Balasubramaniam, V. M.; Ting, E. Y.; Stewart, C. M.; Robbins, J. A. Recommended Laboratory Practices for Conducting High-Pressure Microbial Inactivation Experiments. *Innov. Food Sci. Emerg. Technol.* **2004**, *5*, 299−306.
(95) Bruins, M. E.; Matser, A. M.; Janssen, A. E. M.; Boom, R. M. Buffer Select increasing Pon for HP Treatment of Biomaterials and Its Consequences for Enzyme Inactivation Studies. *High Press. Res.* **2007**, *27*, 101−107.
(96) Kolhe, P.; Amend, E.; Singh, S. K. Impact of Freezing on PH of Buffered Solutions and Consequences for Monoclonal Antibody Aggregation. *Biotechnol. Prog.* **2010**, *26*, 727−733.
(97) Howlett, J. R.; Ismail, A. A.; Armstrong, D. W.; Wong, P. T. T. Pressure-Induced Conformational Changes in an Antigen and an Antibody and the Implications on Their Use for Hyperbaric Immunoadsorption. *Biochim. Biophys. Acta, Protein Struct. Mol. Enzymol.* **1992**, *1159*, 227−236.

https://doi.org/10.1021/acs.molpharmaceut.1c00604
Mol. Pharmaceutics 2021, 18, 4415−4427